

The dark haloes of early-type galaxies in low-density environments: XMM-Newton and Chandra observations of NGC 57, NGC 7796 and IC 1531^{*}

Ewan O’Sullivan^{†1}, Alastair J. R. Sanderson² and Trevor J. Ponman²

¹ *Harvard-Smithsonian Center for Astrophysics, 60 Garden Street, Cambridge, MA 02138*

² *School of Physics and Astronomy, University of Birmingham, Edgbaston, B15 2TT, UK*

Accepted 2007 July 11. Received 2007 July 10; in original form 2007 March 30

ABSTRACT

We present analysis of *Chandra* and *XMM-Newton* observations of three early-type galaxies, NGC 57, NGC 7796 and IC 1531. All three are found in very low density environments, and appear to have no neighbours of comparable size. NGC 57 has a halo of $kT \sim 0.9$ keV, solar metallicity gas, while NGC 7796 and IC 1531 both have ~ 0.55 keV, 0.5 – $0.6 Z_{\odot}$ haloes. IC 1531 has a relatively compact halo, and we consider it likely that gas has been removed from the system by the effects of AGN heating. For NGC 57 and NGC 7796 we estimate mass, entropy and cooling time profiles and find that NGC 57 has a fairly massive dark halo with a mass-to-light ratio of $44.7_{-8.5}^{+4.0} M_{\odot}/L_{B\odot}$ (1σ uncertainties) at $4.75r_e$. This is very similar to the mass-to-light ratio found for NGC 4555 and confirms that isolated ellipticals can possess sizable dark matter haloes. We find a significantly lower mass-to-light ratio for NGC 7796, $10.6_{-2.3}^{+2.5} M_{\odot}/L_{B\odot}$ at $5r_e$, and discuss the possibility that NGC 7796 hosts a galactic wind, causing us to underestimate its mass.

Key words: galaxies: elliptical and lenticular, cD — galaxies: individual: NGC 57, IC 1531 and NGC 7796 — X-rays: galaxies

1 INTRODUCTION

While the majority of early-type galaxies are found in groups and clusters (Tully 1987; Melnick & Sargent 1977; Dressler 1980), there is reason to believe that these environments may not be best choice for studies of intrinsic galaxy properties. The low velocities and high densities of galaxy groups are conducive to galaxy merging, and simulations suggest that gravitational encounters between galaxies can lead to the loss of dark matter (DM) to the surrounding group or cluster halo (Barnes 1989). X-ray observations have shown that the potential wells of groups and clusters are commonly filled with haloes of high temperature gas (Kellogg et al. 1975). Elliptical galaxies are also known to possess such gaseous haloes (Forman et al. 1985; Trinchieri et al. 1986). As well as the inevitable confusion caused by attempting to observe a galaxy halo through surrounding cluster gas, ram-pressure and viscous stripping may remove gas from individual galaxies as they move through the intra-cluster medium (ICM, e.g. Acreman et al. 2003). Models of massive galaxies in the cores of larger systems suggest that their haloes may be enhanced by the inflow of gas from

the surrounding intracluster medium (Mathews & Brighenti 2003). However, the dominant elliptical galaxies of clusters and groups are known to be the most X-ray luminous examples of their type (Helsdon et al. 2001; O’Sullivan et al. 2001), and so are often chosen for the most detailed X-ray analysis. While very high quality can be obtained from such observations, they can only be at best a doubtful source of information on the inherent X-ray properties of early-type galaxies.

One motivation for examining the gas haloes of early-type galaxies is that, under the assumption that they are in hydrostatic equilibrium, it is possible to use them to infer the total mass profile of the galaxy. This feature has become particularly important recently, owing to reports that some ellipticals may contain little or no dark matter (Romanowsky et al. 2003), based on modelling of the kinematics of their planetary nebula population. These have provoked discussion of the potential biases affecting different dynamical mass estimation techniques (e.g. Dekel et al. 2005; Mamon & Łokas 2005a; Douglas et al. 2007). Dynamical mass measurements at large radii rest on modelling of the velocity field of planetary nebulae or globular clusters, which may be affected by a number of factors, most notably orbital anisotropy, flattening of the galaxy along the line of sight, and the assumed link between planetary nebulae and the old stellar population, which is uncertain.

Given the uncertainties associated with kinematical mod-

^{*} Based on observations obtained with XMM-Newton, an ESA science mission with instruments and contributions directly funded by ESA Member States and NASA.

[†] E-mail: eosullivan@head.cfa.harvard.edu

elling, mass profiles based on X-ray observations can potentially provide a much needed independent measurement of DM content. However, as described above, group and cluster environments may affect the properties of member galaxies and introduce confusion to observations. Isolated ellipticals are therefore preferable for this type of study. Mass estimation in the inner regions of ellipticals may also be biased by pressure fluctuations induced by energy injection from an active nucleus. Analysis of *Chandra* observations of a number of ellipticals shows that their optical and X-ray morphologies are uncorrelated within 1.2 optical effective radii (Diehl & Statler 2006). As the mass within this radius should be completely dominated by the stellar contribution, the lack of correlation suggests that the gas is not in hydrostatic equilibrium, with AGN activity the most likely culprit. For low mass or dynamically young ellipticals there is also the possibility that the X-ray emitting gas may take the form of a wind rather than a hydrostatic halo. This has been demonstrated in detail for NGC 3379, where X-ray and dynamical mass estimates disagree strongly (Pellegrini & Ciotti 2006). Modelling as an outflowing wind with properties determined by the rate of supernova heating as well as the mass profile produces a closer agreement. We therefore need to exercise caution when choosing ellipticals for study and when interpreting the results, to account for the potential errors introduced by gas motions and AGN heating, particularly in lower mass systems.

In a previous paper (O’Sullivan & Ponman 2004, hereafter referred to as OP04), we discussed a *Chandra* observation of NGC 4555, an isolated elliptical galaxy with an extended X-ray halo, and showed that it possessed a dark matter halo. In this paper we examine *XMM-Newton* and *Chandra* observations of three other early-type galaxies in low-density environments, NGC 57, NGC 7796 and IC 1531. All three galaxies were selected using the same strict isolation criteria used to identify NGC 4555 (discussed in § 4), and NGC 57 has been identified as isolated by other surveys (Smith et al. 2004). IC 1531 hosts a fairly bright extended radio source (Ekers et al. 1989) apparently associated with the active nucleus of the galaxy. NGC 57 and NGC 7796 have no known radio sources associated with them. None of the galaxies have been extensively studied in the X-ray, and optical data for NGC 57 and IC 1531 are sparse. Bertin et al. (1994) found NGC 7796 to be a boxy elliptical with a small rotational velocity and flat velocity dispersion profile. The galaxy does possess a counter-rotating core inside $4''$, consisting of old, α -element enhanced stars (Milone et al. 2007), perhaps indicating a past interaction or merger. Despite this, NGC 7796 lies on the Fundamental Plane (Reda et al. 2005), suggesting that the stellar component is relaxed, and has a luminosity weighted age of 11.8 ± 1.9 Gyr (Thomas et al. 2005).

Some basic details of the three galaxies are given in Table 1. For NGC 57 and IC 1531 we take distances and luminosities from O’Sullivan et al. (2001). For NGC 7796 we adopt the surface brightness fluctuation distance from Tonry et al. (2001), corrected to match the Cepheid zero point of Freedman et al. (2001) as described in Jensen et al. (2003). We correct the O’Sullivan et al. (2001) optical luminosity to match this distance. Throughout this paper we assume $H_0 = 75 \text{ km s}^{-1} \text{ Mpc}^{-1}$, consistent with the WMAP 3-year mean value of $74 \pm 3 \text{ km s}^{-1} \text{ Mpc}^{-1}$ (Spergel et al. 2007), and normalize optical *B*-Band luminosities to the *B*-band luminosity of the sun, $L_{B\odot} = 5.2 \times 10^{32} \text{ erg s}^{-1}$. Abundances are measured relative to the solar abundance ratios of Grevesse & Sauval (1998), which differ from the older ratios of Anders & Grevesse (1989) primarily in that they use an abundance of Fe a factor of ~ 1.4 lower.

Galaxy	NGC 57	IC 1531	NGC 7796
R.A. (J2000)	00 ^h 15 ^m 30 ^s .9	00 ^h 09 ^m 35 ^s .5	23 ^h 58 ^m 59 ^s .8
Dec. (J2000)	+17°19′42″	-32°16′37″	-55°27′30″
Redshift	0.0181	0.0256	0.0110
Distance (Mpc)	72.53	109.81	46.34
l' (kpc)	21.10	31.94	13.48
D_{25} radius (kpc)	25.31	27.14	15.09
N_{H} (cm^{-2})	4.01×10^{20}	1.35×10^{20}	2.25×10^{20}
Log L_{B} ($L_{B\odot}$)	10.61	10.87	10.62
<i>XMM</i> ObsID	0202190201	0202190301	-
<i>Chandra</i> ObsID	-	5783	7061,7041

Table 1. Location and scale of the three galaxies, and ObIDs for the X-ray exposures used in each case.

2 OBSERVATIONS AND DATA ANALYSIS

NGC 57 and IC 1531 were observed by *XMM-Newton* during orbits 737 (2003 December 17-18, ObsID 0202190201) and 814 (2004 May 20, ObsID 0202190301), for ~ 28.6 ks and ~ 24.6 ks respectively. A detailed summary of the *XMM-Newton* mission and instrumentation can be found in Jansen et al. (2001), and references therein. In both cases, the EPIC MOS and PN instruments were operated in full frame and extended full frame mode, with the medium filter. The raw data from the EPIC instruments were processed with the *XMM-Newton* Science Analysis System (SAS v. 7.0), using the `epchain` and `emchain` tasks. After filtering for bad pixels and columns, X-ray events corresponding to patterns 0-12 for the two MOS cameras and patterns 0-4 for the PN camera were accepted. Both observations suffered from mild background flaring, and times when the total count rate deviated from the mean by more than 3σ were therefore excluded. The effective exposure times for the MOS 1, MOS 2 and PN cameras were 21.2, 21.1 and 18.7 ks respectively for NGC 57 and 16.2, 16.3 and 11.7 ks for IC 1531.

Images and spectra were extracted, responses generated, and point sources removed as described in O’Sullivan et al. (2005). NGC 57 and IC 1531 cover small enough areas of the field of view that local background spectra can also be used, but we also extracted background images and spectra as described in O’Sullivan et al. (2007), using the “double-subtraction” method (Arnaud et al. 2002; Pratt et al. 2001). Comparison showed little difference between the alternative background spectra. The local background spectra were used in spectral fitting, and produced generally acceptable results.

IC 1531 and NGC 7796 were observed by *Chandra* on 2005 August 21 for ~ 40 ksec (IC 1531) and on 2006 August 28 and 2006 September 03 for ~ 54 and ~ 20 ksec (NGC 7796), with ACIS operating in Very Faint mode (ObsIDs 5783, 7061 and 7401). A summary of the *Chandra* mission and instrumentation can be found in Weisskopf et al. (2002). The S3 chip was at the telescope focus. Reduction and analysis were performed using methods similar to those described in OP04. The level 1 events file was reprocessed using CIAO v3.3 and CALDB v3.2.1 (Fruscione et al. 2006). Bad pixels and events with ASCA grades 1, 5 and 7 were removed. The data were corrected to the appropriate gain map, the standard time-dependent gain correction was made, and a background light curve was produced. A background flare occurred toward the end of the IC 1531 exposure and all periods where the count rate deviated from the mean by $> 3\sigma$ were excluded, leaving a clean exposure time of 30.7 ksec. In the case of NGC 7796, only minor variations were found in the background, and the useful exposure times were 52.2 ksec and 17.6 ksec. As the two exposures were taken only a few days apart and have identical instrumental setup, we merged

the events lists before further analysis. Subsequent comparison of results from the merged data and individual exposures shows no significant differences. In all cases, We chose to use data from the S3 chip only, as the sources are relatively compact and do not produce any useful flux on the neighbouring chips.

Point sources were identified using the CIAO task `wavdetect` with a detection threshold chosen to ensure ≤ 1 false source in the field. Source ellipses with axes 8 times the standard deviation of the source distribution were used to exclude the point sources, with the exception of a source coincident with the optical centre of IC 1531. Images and spectra were extracted from the cleaned data, and exposure maps and weighted responses extracted as described in the CIAO threads¹.

CIAO v3.4 and CALDB v3.3 were released during our analysis of the *Chandra* data. To test the effect of the improved calibration and handling of serial charge transfer inefficiency (CTI) on our results, we reprocessed the NGC 7796 observations using the more recent software and extracted spectra. We found that the correction for serial CTI increased the number of counts in the energy range 0.3-7.0 keV in the S3 chip by $\sim 1\%$. Spectral fitting produced almost identical results, with gas temperatures changing by ~ 0.01 keV. We therefore concluded that our original analysis was satisfactory and unlikely to be significantly improved by using the improved software.

3 RESULTS

Figure 1 shows exposure and vignetting corrected adaptively smoothed images of the three galaxies. *XMM-Newton* data are used for NGC 57 and IC 1531, combining data from the MOS and PN cameras. Smoothing was carried out with the SAS `asmooth` task, with smoothing scales chosen to achieve a signal-to-noise ratio of 10. NVSS radio contours are overlaid on the image of IC 1531. The combined ACIS-S3 data are used for NGC 7796, and smoothing is performed with the CIAO `smooth` task with signal-to-noise of 3-5. All three galaxies have relatively compact X-ray emission, extending to only a little further than the D_{25} ellipse (which approximates the 25 mag/arcsecond optical isophote). The surrounding fields show a number of point sources, and there is also an apparently diffuse feature to the southwest of NGC 57 (marked with a white cross), which will be referred to hereafter as XMMU J001526.4+171723.

3.1 Surface brightness models

We prepared images of all three galaxies in the 0.3-2.0 keV band, with point sources removed. The energy band was chosen to maximize the signal-to-noise ratio for gaseous emission in the sources. Appropriate exposure maps were generated for each image. In the case of the *XMM* data, PSF images were also created and as the number of detected counts from each camera was relatively low, we summed the *XMM* images and associated exposure maps and PSFs from all three cameras to produce a single set of products for each galaxy. The images were binned to the EPIC-PN physical pixel size of $4.4''$. For *Chandra*, the $0.49''$ physical pixel size was used, and we ignored the PSF as it is comparable to the pixel

Parameter	NGC 57	IC 1531	NGC 7796
r_{core} ($''$)	$5.33^{+0.36}_{-5.33}$	$1.03^{+0.33}_{-0.53}$	$0.35^{+0.28}_{-0.21}$
β_{fit}	$0.594^{+0.047}_{-0.109}$	$0.582^{+0.009}_{-0.11}$	$0.390^{+0.008}_{-0.011}$
$r_{core,2}$ ($''$)	-	-	$3.10^{+26.3}_{-3.1}$
$\beta_{fit,2}$	-	-	$0.963^{+1.046}_{-0.278}$

Table 2. Best fitting beta model parameters and 1σ errors from the surface brightness fits to the three galaxies. The model fit to NGC 57 also included a point source component.

scale. Fitting was performed in the CIAO SHERPA package. As accurate *XMM* fitting requires PSF convolution and the SHERPA one-dimensional PSF convolution is known to be inaccurate, all *XMM* fits were performed comparing models directly to the images. For fits to *Chandra* data alone, 1-D fits to the exposure-corrected data are generally acceptable. As the galaxies occupy relatively small areas near the focus of each camera, we assumed the background to be flat (after exposure correction) and included an appropriate model component to account for its contribution. For 2-D fits, as the source images have many pixels with few counts (or none), we used the Cash statistic (Cash 1979) when fitting. This statistic only provides a relative measure of the goodness of fit, so that while it allows us to improve fits and find the best solution for a given model, it gives no information on the absolute goodness of the final fit. We therefore use azimuthally averaged radial profiles and residual images to help determine whether particular fits are acceptable. Figure 2 shows radial profiles of our best fits to each galaxy, and table 2 shows the best fitting parameters for the models used.

We found that for IC 1531 the source was only marginally extended in the *XMM* data, and therefore difficult to fit accurately. We therefore fit the *Chandra* data only. IC 1531 hosts a bright radio source (0.48 Jy at 2.7 GHz, Ekers et al. 1989) which extends ~ 200 kpc south-east (see Figure 1). The *Chandra* data reveals a central X-ray source with a jet-like extension of a few pixels with a similar orientation to the radio extension axis. Fitting with the central source included, we found that the radial profile was best fit by a beta model with no point source component, as the contribution from the jet mimics an extended central region. The beta model provided a rather poor fit, with clear deviations from the data at both large and small radii. Excluding the inner two bins of the profile, we found that the beta model fit was greatly improved, and we have taken this as our best fit model for this galaxy. Adding a point source with normalization fixed to match the central bin produced only very minor changes in the shape of the beta model (core radius and beta changed by factors similar to their uncertainties), and only significantly affected the normalisation of the model. For NGC 57, we found it necessary to add a point source model in order to achieve a reliable fit. NGC 7796 is moderately well fit by a single beta model, but the fit is improved if a second beta component is added. Comparing the two fits with the F-test, we find a 0.6 per cent probability that the difference in fit statistic is not significant, so we consider the two-beta model to be a significant improvement. We also tried fitting using a beta model with a point source, but the excess emission above the beta model is clearly more extended than would be expected from a point source. We therefore accept the two beta model as the best fit for this galaxy.

3.2 Spectral models

We initially fitted the integrated spectra of each galaxy, using circular extraction regions of radius $150''$ (~ 53 kpc) for NGC 57,

¹ <http://asc.harvard.edu/ciao/threads/index.html>

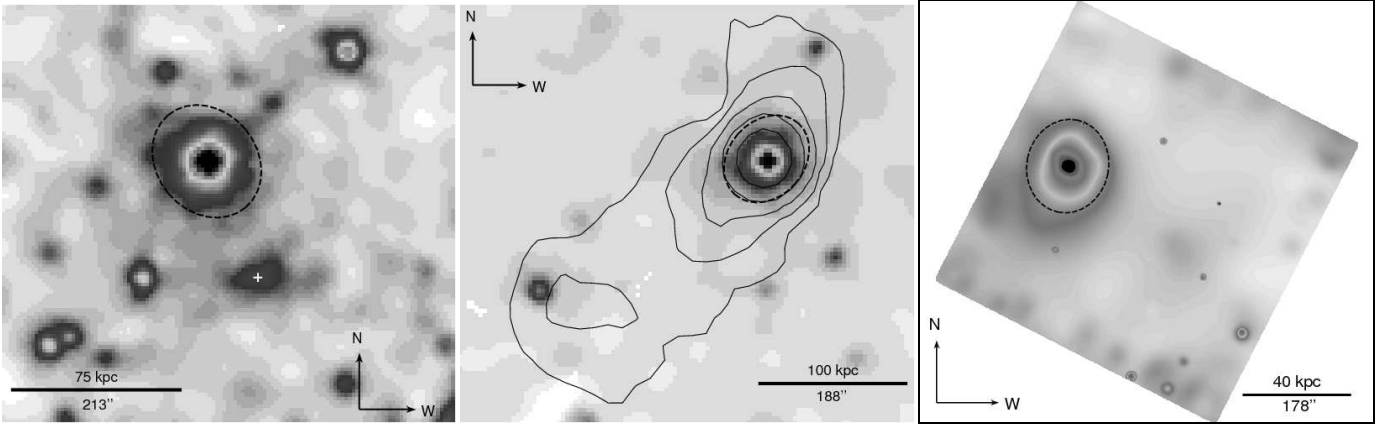


Figure 1. Adaptively smoothed mosaiced 0.3–2.0 keV *XMM* EPIC MOS+PN images of NGC 57 (*left*) and IC 1531 (*centre*), and *Chandra* ACIS-S3 image of NGC 7796 (*right*). NVSS radio contours marking 3, 9, 27, 81 and 243 σ significance are overlaid on the IC 1531 image. Dashed black lines mark the D_{25} ellipse for each galaxy.

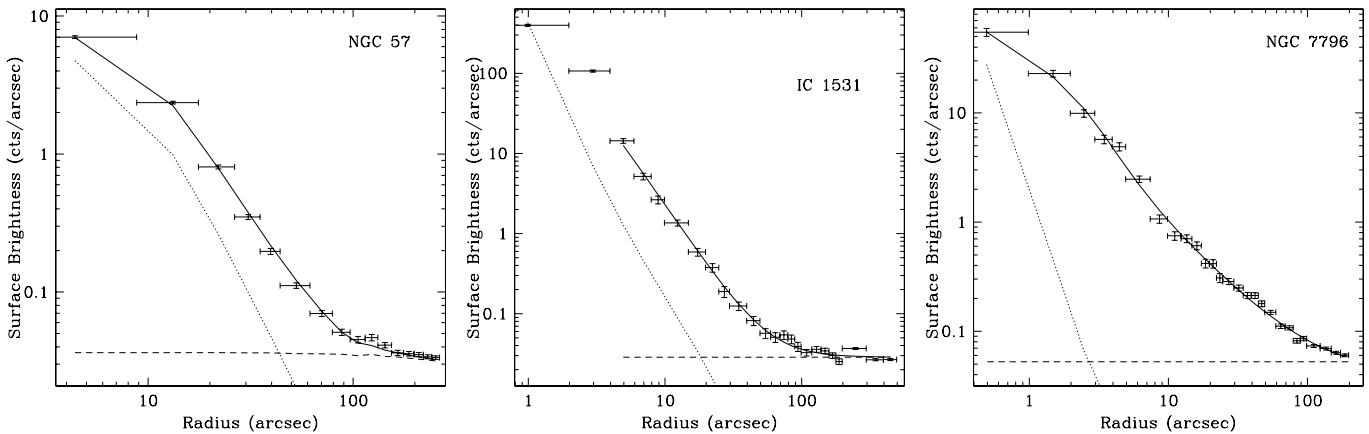


Figure 2. *XMM* radial surface brightness profile of NGC 57 (*left*), and *Chandra* profiles of IC 1531 (*centre*) and NGC 7796 (*right*), showing the data (error bars) best fitting model (solid line) and background (dashed line). The *XMM* and *Chandra* PSFs are marked by dotted lines, but only in the case of NGC 57 was a point source component included in the fit. For IC 1531, the central two bins were excluded from fitting due to contamination by the central point source and jet.

30'' (~ 16 kpc) for IC 1531 and 100'' (~ 24 kpc) for NGC 7796. The radii were selected based on the surface brightness fits to contain all the detected diffuse emission associated with each galaxy. Nearby point sources were excluded and, in the case of NGC 57, a region to the southwest corresponding to the diffuse feature marked in Figure 1. The region used to exclude this feature was a circle of radius $\sim 47''$ centred at $00^{\text{h}}15^{\text{m}}16^{\text{s}}.2 +00^{\circ}17'20''$. Source and background spectra were extracted, appropriate responses created, and the source spectra grouped to 20 counts per bin. The spectra were fitted using *XSPEC* v. 11.3.2z, ignoring energies lower than 0.4 keV and higher than 7.0 keV. Hydrogen column was held fixed at the galactic value in all cases. For NGC 57 and IC 1531, we simultaneously fit spectra from all three *XMM* EPIC cameras. The *Chandra* spectrum for IC 1531 was fitted independently as a check on the *XMM* fits. For NGC 7796 we simultaneously fitted spectra drawn from the two observations. Experimentation showed that independent fits to each spectra produced consistent results, though with large errors in the case of the shorter exposure.

For NGC 57 we found that the spectrum could be fit using a single temperature APEC plasma model (Smith et al. 2001), with a powerlaw component presumably describing emission from un-

resolved point sources and the AGN. However, residuals above and below the Fe peak at ~ 1 keV indicated that the fit might be improved by the addition of a second plasma component (Buote & Fabian 1998; Buote 2000). This two-temperature model did produce a somewhat better fit, though with less well constrained errors on some of the parameters. The results of both fits are shown in Table 3. We also tried fits in which individual elemental abundances were allowed to vary freely, but found no significant improvement. Similar fits to the *XMM* data for IC 1531 showed that this object has a much higher contribution (79 per cent) to its total emission from the powerlaw component. From the surface brightness models, we can estimate the fraction of powerlaw emission expected from a point source with normalisation chosen to match the central surface brightness bin to be ~ 85 per cent. Given the uncertainties involved, this seems a reasonable agreement. Considering its strong radio emission, we believe that the central AGN is the dominant source of X-ray emission in the IC 1531. A single temperature fit was found to be acceptable for this galaxy, and is shown in Table 3. For NGC 7796, a single temperature plasma model with a powerlaw component was also found to be acceptable, and addition of a second plasma component produced no sig-

Galaxy	Model	kT (keV)	kT2 (keV)	Z (Z_{\odot})	red. χ^2	d.o.f.	Flux ($\text{erg s}^{-1} \text{cm}^{-2}$)	Fraction $_{PL}$	$L_{X,gas}$
NGC 57	1T+PL	0.93 ± 0.02	-	$0.97^{+0.86}_{-0.44}$	1.111	346	4.710×10^{-13}	0.60/-/0.40	1.78×10^{41}
NGC 57	2T+PL	0.83 ± 0.02	$1.79^{+0.54}_{-0.32}$	$1.31^{+0.40}_{-0.43}$	0.994	344	4.640×10^{-13}	0.51/0.26/0.23	2.24×10^{41}
IC 1531	1T+PL	0.55 ± 0.03	-	$0.61^{+0.11}_{-0.08}$	0.895	299	4.645×10^{-13}	0.21/-/0.79	1.41×10^{41}
NGC 7796	1T+PL	0.53 ± 0.03	-	$0.53^{+4.33}_{-0.13}$	1.036	194	3.205×10^{-13}	0.76/-/0.24	7.24×10^{40}

Table 3. Best fit models to integrated *XMM* spectra. Spectral models consist of powerlaw (PL) and either single temperature (1T) or two-temperature (2T) APEC components. 90% errors are given and fluxes are calculated for the 0.4–7.0 keV band. The fraction $_{PL}$ entry shows the fraction of flux produced by each model component, in (APEC/APEC/powerlaw) order. All fits were performed with N_{H} fixed at the galactic value.

nificant improvement in the fit. However, in this case the plasma component produces the majority of the flux.

As the emission from IC 1531 is largely confined within $30''$ of the galaxy centre and is dominated by emission from the AGN, we do not attempt to split the *XMM* data for this galaxy into radial bins. With the higher spatial resolution *Chandra* data we were able to extract spectra from two regions, a central circular region within $7.5''$ and an outer annulus with radius $7.5\text{--}30''$. The central region completely encloses the central point source and jet structure and we expect it to be dominated by the AGN. Fitting with an APEC+Powerlaw model, we found a similar temperature for the plasma component to that measured from the *XMM* data ($0.55^{+0.06}_{-0.07}$ keV). Abundance was essentially unconstrained, probably due to trade-offs against the normalizations of the powerlaw and APEC models. The powerlaw dominated the emission, producing $\sim 90\%$ of the 0.4–7.0 keV flux, for a total luminosity of $2.90^{+0.15}_{-0.29} \times 10^{41} \text{ erg s}^{-1}$, which can be considered as an upper limit on the X-ray emission of the AGN. For the outer region, the gas temperature was marginally lower ($0.52^{+0.05}_{-0.07}$ keV) and abundance only poorly constrained ($0.44^{+0.51}_{-0.28} Z_{\odot}$). There is still a strong powerlaw component in this region, contributing about one third of the total flux. This probably consists of emission from the X-ray binary population of the galaxy.

NGC 7796 is more extended than IC 1531 and we were able to split the emission into four radial bins with outer radii $10''$, $30''$, $50''$ and $100''$ (~ 2.5 , 7, 12 and 24 kpc). We fitted APEC+powerlaw models, but found that the powerlaw component was only required in the inner two bins. Abundance proved to be poorly constrained in all bins, owing to the trade-offs against the powerlaw component and poor statistics. However temperature was well constrained and was not affected by leaving abundance free or fixing it at the value derived from the integrated spectrum. Figure 3 shows the temperature profile of NGC 7796. All four bins have best-fitting temperatures of between 0.48 and 0.58 keV, with errors of 0.05 keV or less. No trend in temperature with radius was found, and the radial temperature profile agreed closely with the temperature measured from the integrated spectrum.

NGC 57 has sufficiently extended emission to allow us to extract spectra in three concentric circular annuli with outer radii $30''$, $80''$, and $150''$ (~ 10 , 28 and 53 kpc). We again fitted APEC+powerlaw models, and results from these fits are shown in Figure 4. Fit quality is similar in all three bins, with reduced χ^2 0.95–1.15. In the central bin, this can be improved by the addition of a second APEC model, which gives reduced $\chi^2=1.02$. The high value of the abundance in the two-temperature model and its large errors may be an indication that the data are too poor to support such a complex model rather than an indication of a real 2–2.5 Z_{\odot} abundance in the galaxy core. There are indications of an abundance gradient in the galaxy, but the errors are large enough that we cannot confirm this. The galaxy halo appears to be approxi-

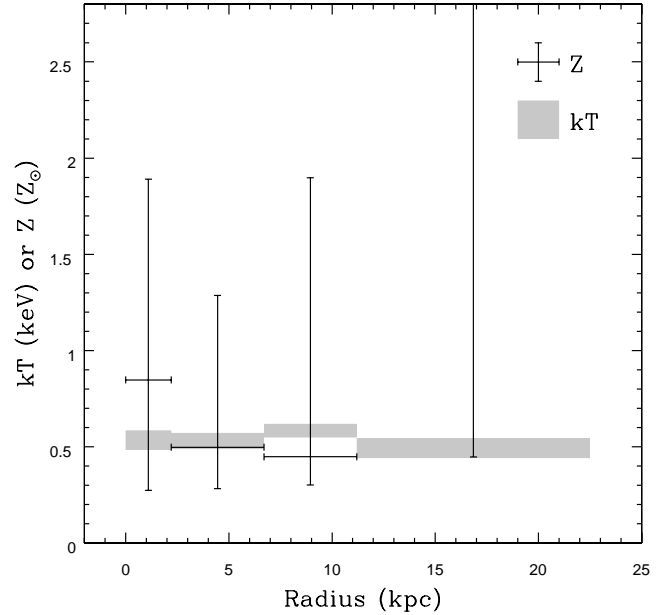


Figure 3. Temperature and abundance profiles for NGC 7796. 90% error regions are indicated by the symbols. The abundance of the outermost bin is essentially unconstrained.

mately isothermal, with a possible slight fall in temperature in the core. This could be an indication of radiative cooling in action in the densest parts of the galaxy halo, but the difference is small, so the assumption of isothermality is reasonable.

3.3 XMMU J001526.4+171723

As mentioned previously, there is a small area of apparently diffuse emission $\sim 2.5'$ to the southwest of NGC 57. The NASA/IPAC extragalactic Database (NED) contains no object at this position, and the nearest known extragalactic object is in fact NGC 57. Examination of the Digitized Sky Survey (DSS) images for this position shows only very faint sources with too little detail to allow identification. Comparison with the PSF of the three *XMM* telescopes at this off axis angle shows that the source is definitely extended. In total, XMMU J001526.4+171723 contains ~ 530 counts, enough for a crude spectral fit. However, the two MOS cameras contain only ~ 120 counts each and therefore provide very poor spectra. We therefore fit models simultaneously to all three cameras, and to the PN alone. The results of these fits can be seen in Table 4.

These fits are clearly poorly constrained by the data, but it appears that a powerlaw is a significantly worse description of the PN data. The abundance of the plasma models is $< 0.06 Z_{\odot}$ at the

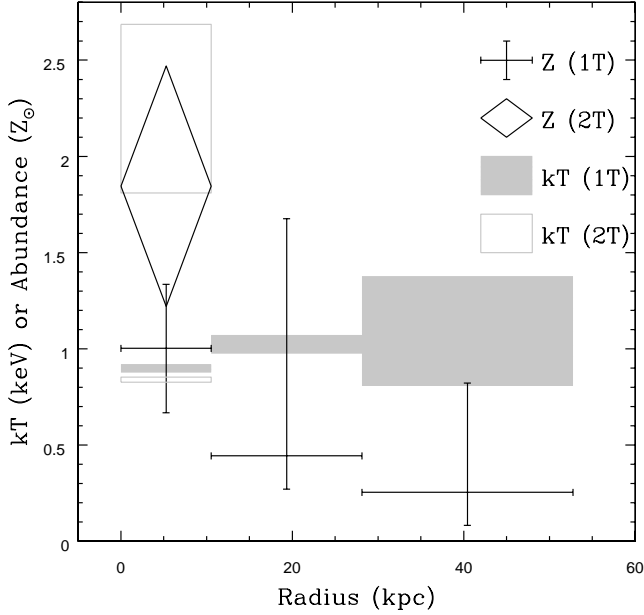


Figure 4. Temperature and Abundance profiles for NGC 57. Symbols indicate 90% error regions on the fitted parameters.

Parameter	3 Cameras		PN only	
	APEC	Powerlaw	APEC	Powerlaw
kT (keV)	1.38 ^{+0.61} _{-0.41}	-	0.91 ^{+0.58} _{-0.27}	-
Z (Z_{\odot})	0.01 ^{+0.09} _{-0.01}	-	0.01 ^{+0.05} _{-0.01}	-
Γ	-	2.27 ^{+0.28} _{-0.26}	-	2.30 ^{+0.35} _{-0.31}
red. χ^2	1.19	1.16	0.873	1.107
d.o.f.	19	20	10	17
Flux ($\times 10^{-14}$ erg s ⁻¹ cm ⁻²)	2.07	2.49	2.05	2.47

Table 4. Spectral fits to source XMMU J001526.4+171723.

90% level, but it should be noted that for low temperature sources, fitting a single temperature model to a source consisting of a multi-temperature plasma is likely to produce systematically low abundances (Buote & Fabian 1998; Buote 2000). We therefore consider it fair to characterise the source as an extended object with a temperature of ~ 0.9 - 1.3 keV, flux of 2 - 2.5×10^{-14} erg s⁻¹ cm⁻², and possibly a low abundance.

The most likely explanations of this source are that it is associated with NGC 57, or that it is a background object which happens to lie close to our target galaxy. While the temperature of XMMU J001526.4+171723 is similar to that of the plasma component of NGC 57, the measured abundance is quite different, even considering the large errors associated with both abundance measurements. Given the isolation of NGC 57, which suggests that it is unlikely to have undergone any significant interaction in its recent history, it is difficult to explain the presence of a large cloud of X-ray temperature gas separated from the main galaxy halo, with no associated stellar component. If XMMU J001526.4+171723 were at the same distance as NGC 57, it would be ~ 20 kpc in diameter, separated from the galaxy halo by ~ 30 kpc, and would have a luminosity of 1.34 - 1.96×10^{40} erg s⁻¹. Assuming it to be a sphere of uniform density (as a first approximation), it would contain ~ 3.2 - $3.5 \times 10^8 M_{\odot}$. This is comparable to the hot gas content of a galaxy.

If XMMU J001526.4+171723 is a background object, we can place constraints on its distance from the spectral fits. Given the temperature of the system, it would most likely be a galaxy group or poor cluster. Allowing redshift to vary as part of the PN spectral fit gives a 90% upper limit on redshift of ~ 0.32 . This is equivalent to an angular size distance $D_A = 902.5$ Mpc and a luminosity distance $D_L = 1572.5$ Mpc, suggesting that the source is ~ 125 kpc in radius and has a luminosity of 6.3 - 9.2×10^{42} erg s⁻¹. These values seem quite reasonable for a large galaxy group. Alternatively, we can assume an upper limit on X-ray luminosity of 10^{43} erg s⁻¹, from which we estimate $D_L < 1980.9$ Mpc, equivalent to a redshift of ~ 0.39 . At this redshift, the system would have a radius of 140 kpc, again quite compatible with a poor cluster. We can estimate the apparent magnitude of the dominant galaxy of such a system, under the assumption that it has a luminosity of 3 - $10 \times 10^{10} L_{\odot}$, typical of a giant elliptical or cD galaxy. Using a redshift of 0.32, this is equivalent to an apparent magnitude of ~ 19.0 - 20.2 . Although this approaches the limiting magnitude of the DSS plates, it is perhaps a little surprising that we do not see any more obvious galaxy candidates.

3.4 Mass, entropy, and cooling time

Given the density and temperature distribution of a gaseous halo, it is possible to estimate a number of three dimensional properties such as mass, entropy and cooling time. For both NGC 57 and NGC 7796 we can approximate the temperature structure as isothermal, fitting a constant temperature model to our radial temperature profiles, and calculate the density profile based on our surface brightness models. Unfortunately, for IC 1531 we believe the data are too poor to support such an analysis. The presence of a powerful radio/X-ray jet source suggests the possibility of interactions between jet and gas which could mean that the gas is out of hydrostatic equilibrium. The compactness of the region from which we detect gas emission (~ 16 kpc radius) is not what we would expect for a system with a relaxed hydrostatic halo. We therefore exclude IC 1531 the following analysis.

We can use the well known equation for hydrostatic equilibrium,

$$M_{tot}(< r) = -\frac{kTr}{\mu m_p G} \left(\frac{d \ln \rho_{gas}}{d \ln r} + \frac{d \ln T}{d \ln r} \right), \quad (1)$$

to calculate the total mass within a given radius. From density, temperature and total mass, we can calculate parameters such as gas fraction, cooling time and entropy where entropy is defined to be

$$S = \frac{T}{n_e^{\frac{2}{3}}}. \quad (2)$$

We estimate the errors on the derived values using a monte-carlo technique. The known errors on the temperature and surface brightness models, and on other factors such as the total luminosity, are used to randomly vary the input parameters. We then generate 10000 realisations of the derived parameters profiles, and use these to calculate the 1σ error on each parameter at any given radius.

We find close agreement between our fits to the radial temperature profiles and the single temperature fits to the integrated spectra. Figure 5 shows the resulting profiles, overplotted for comparison on similar profiles for the isolated elliptical NGC 4555 (from OP04). The outer limit of the plots is determined by the radius to which we can measure the temperature, and the inner limit is set to be half the width of the central temperature bin. The temperature profile of NGC 4555 extends further than that of NGC 57 which is

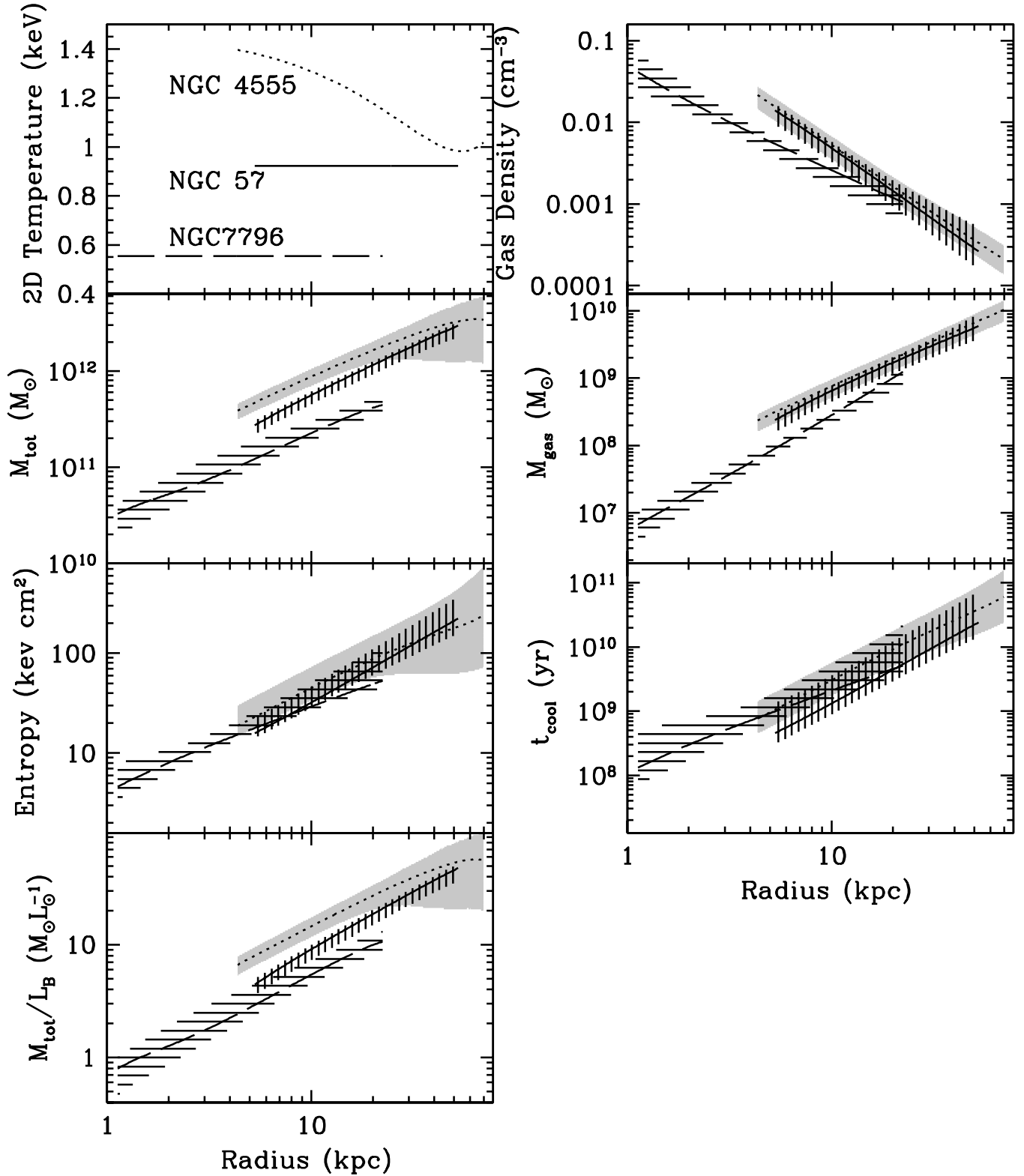


Figure 5. Profiles of mass, gas mass, entropy, cooling time, etc., for NGC 57 and NGC 7796, with similar profiles for NGC 4555 plotted for comparison. The dotted line and grey shading show the best fit and 1σ error regions for NGC 4555, the solid line and vertically hatched area NGC 57 and the dashed line and horizontal hatching NGC 7796.

itself more extended than NGC 7796, although we have finer detail in the core of the latter galaxy.

We note that because we are using an isothermal approximation of the temperature, the uncertainty of the temperature model is constant with radius. In the case of NGC 7796 this agrees relatively well with the results of the radial temperature profile, but for NGC 57 the approximation does not reflect the larger uncertainty in the outermost temperature bin. As the total mass is largely determined by the temperature model, the resulting uncertainty on the total mass for NGC 57 is also constant with radius. Our choice of assumptions may underestimate the true uncertainty on total mass; we therefore repeated the analysis using a simple temperature gradient rather than an isothermal model in order to test whether this significantly altered the mass profile. The resulting best fitting total mass is a factor of 1.1 larger, with uncertainties a factor ~ 1.5 larger.

To calculate the mass-to-light ratio, we use B band effective radii for the two galaxies (33.1'' for NGC 57, 25.2'' for NGC 7796; Bacon et al. 1985; Reda et al. 2005), assume that the stellar light profile obeys the standard $r^{1/4}$ law, and normalise the profile by the total B band luminosity. The assumption of $r^{1/4}$ profiles is supported by the fits used to estimate the effective radii. For NGC 57, the mass-to-light ratio at the inner limit of our calculated profile falls to ~ 4 , somewhat lower than the usual assumed stellar mass-to-light ratio of 5-8. However, the total mass-to-light ratio within 55 kpc is $48.38_{-10.30}^{+4.66} M_{\odot}/L_{\odot}$. The mass-to-light ratio of NGC 57 has been previously estimated from the stellar velocity dispersion in the core of the galaxy to be 34.40 ± 0.33 (Bacon et al. 1985), assuming the stellar orbits to be isotropic. This is comparable with the values we find at ~ 30 -40 kpc.

NGC 7796 has a lower temperature than NGC 57 and NGC 4555, and a lower total mass and gas mass at all radii. The M/L ratio is lower than that expected for stars alone within ~ 10 kpc. At the maximum radius to which we can trace the galaxy halo, M/L is a factor of ~ 2 -3 lower than that found for NGC 57 and NGC 4555 at the same radius. A M/L ratio profile based on stellar velocity dispersion measurements (Bertin et al. 1994) has a flatter slope than our profile and finds M/L larger than our estimate for radii between ~ 1 -10 kpc. It therefore seems possible that our X-ray mass estimates do not reflect the true total mass profile for NGC 7796.

Given the differences in gas mass, total mass and temperature of the three systems, it is notable that they have remarkably similar entropy and cooling time profiles. Within the uncertainties, the profiles are indistinguishable over the majority of the range we cover. Cooling time falls below 10^9 yr within 5-10 kpc, suggesting that some form of heating is required in all cases to prevent excessive cooling. The entropy profiles all fall to less than 20 keV cm^2 in the central regions. In NGC 7796 we are able to trace the entropy profile in to ~ 1 kpc without finding evidence of flattening in the profile. Central entropy cores have been observed in some clusters and it has been suggested that they are evidence that AGN heating provides feedback to balance cooling (Voit & Donahue 2005). The lack of such a core in our galaxies may suggest that no significant outbursts have happened in the recent past, or that the heating mechanism does not efficiently deposit energy at small radii.

4 ENVIRONMENT

NGC 57, NGC 7796 and IC 1531 were chosen as examples of early-type galaxies in very low density environments. The selec-

tion criteria were the same as those used in previous papers (OP04, Reda et al. 2004), which specify that the candidate galaxy should have no neighbours which are:

- (i) within 700 km s^{-1} in recession velocity;
- (ii) within 0.67 Mpc in the plane of the sky;
- (iii) less than 2 B -band magnitudes fainter (B_T).

Galaxies which are members of a Lyon Galaxy Group (Garcia 1993) are also excluded. These conditions are intended to ensure that the candidate galaxies do not lie in any group or cluster, and that any neighbouring galaxies are too small or too distant to have had any significant effect on their evolution or properties. Potentially, these criteria could result in the selection of fossil groups, systems in which all major galaxies have merged to form a single elliptical (Ponman & Bertram 1993; Jones et al. 2003). However, our galaxies are too X-ray faint to fall into this category, having halo luminosities below the minimum value of $L_X = 10^{42} \text{ erg s}^{-1}$ (see § 5.2 for further discussion of this issue). Selection was performed using data from the NASA-IPAC Extragalactic Database (NED) and the Lyon-Meudon Extragalactic Data Archive (LEDA, Paturel et al. 2003), and the results were checked by examination of Digitized Sky Survey (DSS) images of the region surrounding the candidates.

However, since the original selection was performed, both LEDA and NED have expanded as more galaxies are identified and more information becomes available. In particular, IC 1531 lies in a 2dF Galaxy Redshift Survey field (see Colless et al. 2001, for detailed description of the 2dFGRS), which provides us with a much clearer picture of its environment than was previously possible. NGC 7796 is on the border of another 2dFGRS field. Figure 6 shows DSS images of the three targets, with neighbouring galaxies marked.

NGC 57, which does not lie in a redshift survey field, has very few definite neighbours; only three small galaxies are within 0.67 Mpc and 700 km s^{-1} . Between 0.67 and 1 Mpc from NGC 57 are three more galaxies. Two are small, but the third, IC 4, is a spiral galaxy only ~ 1.5 magnitudes fainter than NGC 57. However, the distance between the two is large enough that NGC 57 still meets the isolation criteria. We have also tested the possibility that some of the 107 galaxies without redshifts in the area surrounding NGC 57 might be associated with it, by plotting a radial surface density profile for these objects, shown in Figure 7. If there was an unrecognized galaxy group surrounding NGC 57, we would expect to see a high surface density of galaxies at small radii, falling to lower values at larger distances. We find no such trend, which suggests that there is no larger structure around NGC 57. It should be noted that we have not applied any magnitude cut when selecting the surrounding galaxies. The lack of such a limit makes a direct comparison with similar studies of galaxy surface density (Smith et al. 2004; Reda et al. 2004) impractical. We cannot consider our sample complete, and it is possible that inhomogeneities in the coverage of the field could suppress the signs of structure around NGC 57. However, examination of the DSS image suggests that we are not missing any bright galaxies in the field and that any additional neighbours must be relatively low luminosity galaxies. We therefore believe this elliptical to be truly isolated.

The 2dFGRS field in which NGC 7796 falls covers the lower left quadrant of the area shown in Figure 6. The redshift coverage around the galaxy is therefore very uneven. However, only three galaxies within 1 Mpc on the sky are found to have redshifts within 2000 km s^{-1} , and all three are more than 2 magnitudes fainter in B . Considering the galaxies with no redshift measurements, we again

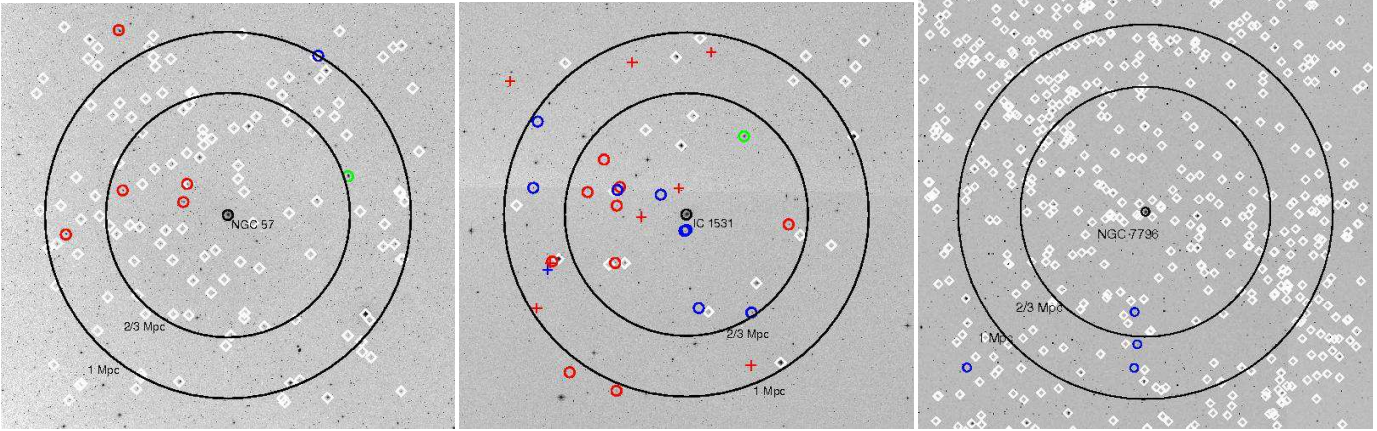


Figure 6. Digitized Sky Survey images of the regions around NGC 57 (*left*), IC 1531 (*centre*) and NGC 7796 (*right*) with the positions of other galaxies marked. Gray diamonds mark galaxies with no measured redshift, red points galaxies with larger recession velocities and blue points those with lower velocities. Green points mark galaxies which are < 2 magnitudes fainter than the target galaxy in B_T . Circles mark galaxies within 700 km s^{-1} of the candidate isolated elliptical and crosses those outside 700 km s^{-1} . Circles marking $2/3$ and 1 Mpc radius at the assumed distance of the candidate are included for scale.

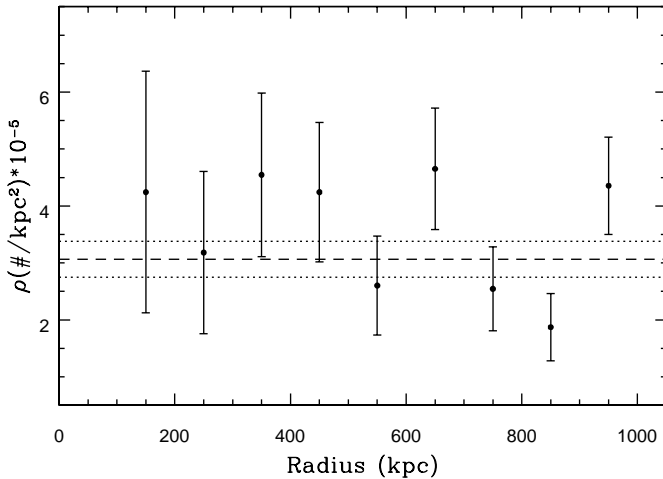


Figure 7. Plots of Surface density of galaxies with no measured redshift surrounding NGC 57. The points show values in bins 100 kpc wide (using the assumed distances of NGC 57), with 1σ error bars. The dashed line shows the best fit constant density model, with dotted lines marking the 1σ errors. 100 kpc is equivalent to $4.74'$.

plot the radial surface density in Figure 7. The surface density appears to be approximately flat out to 1 Mpc , with the exception of the region within 100 kpc of NGC 7796, where we find 7 galaxies. The overdensity suggests that some of these may be satellite galaxies associated with NGC 7796. However, they are very faint; the brightest is 4.2 magnitudes fainter than NGC 7796, equivalent to $L_B = 7.7 \times 10^8 L_{B\odot}$ at the distance of NGC 7796. We therefore conclude that while NGC 7796 may have a small number of companion dwarf ($L_B < 10^9 L_{B\odot}$) galaxies, they are probably too small to have had any significant impact on the formation history of the galaxy. There is no evidence of a group or an extended halo of galaxies around NGC 7796.

IC 1531 is a slightly more difficult case. The 2dFGRS data show there to be a relatively large number of small galaxies in the surrounding area, 13 within 700 km s^{-1} and 0.67 Mpc , 24 within 2000 km s^{-1} and 1 Mpc . One of these galaxies, PGC132744 (also known as 2MASX J00084885-3203089) is an Sc galaxy whose B_T

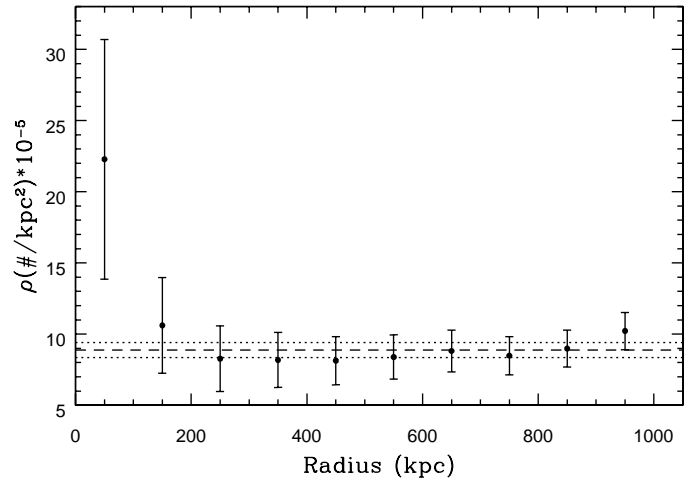


Figure 8. As Figure 7, for the galaxies with no measured redshift around NGC 7796. 100 kpc is equivalent to $6.89'$.

magnitude in LEDA is 15.49 , only 1.65 magnitudes fainter than IC 1531. This means that IC 1531 fails the initial criteria for isolation. However, both galaxies have near infrared magnitudes available, and in J, H and K_S bands, PGC132744 is 3.9 - 4.3 magnitudes fainter than IC 1531. PGC132744 also appears to have a rather clumpy morphology, and its extremely blue colors ($B-K_S = 5.94$) suggests that it may be undergoing a burst of star formation or some other disturbance which has increased its B-band surface brightness. We therefore conclude that IC 1531 should not be ruled out as an isolated elliptical on the basis of this object alone.

Figure 9 shows the distribution of recession velocities for the galaxies in the neighborhood of IC 1531. The galaxies appear to be arranged in two velocity regions, either within $\sim 1000 \text{ km s}^{-1}$ of IC 1531 or in a smaller clump at $\sim 9300 \text{ km s}^{-1}$. However, examination of Figure 6 shows that the galaxies at larger recession velocities are very scattered in the plane of the sky, suggesting that some of them are very distant. Ignoring these objects, we calculate the mean recession velocity of the remaining galaxies to be $\sim 7600 \text{ km s}^{-1}$, only 100 km s^{-1} from the recession ve-

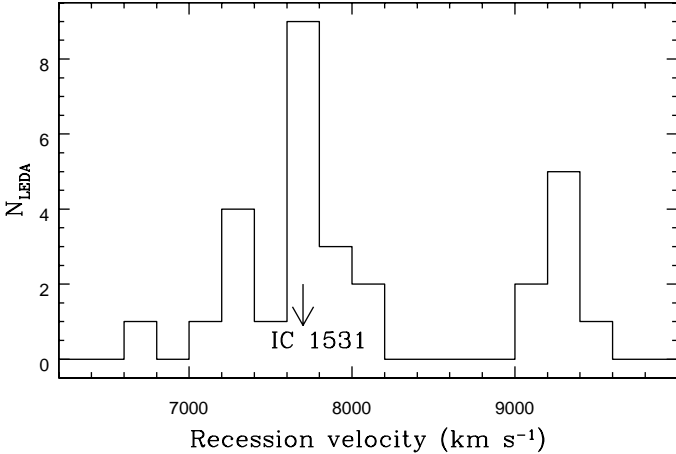


Figure 9. Redshift distribution of the galaxies within 1 Mpc (in the plane of the sky) of IC 1531. The arrow shows the redshift of IC 1531.

locity of IC 1531, with a velocity dispersion of line-of-sight 338 km s^{-1} . With the exception of PGC132744, the galaxies in this velocity grouping have luminosities of $8.5 < \log L_B < 9.6$, so that the brightest of these neighbours is a factor of ~ 18 less luminous than IC 1531, and presumably correspondingly less massive. If we assume that these galaxies form a bound system, we can also estimate the total system mass, using their positions and velocities. We use the Virial theorem and projected mass methods described in Bahcall & Tremaine (1981), and obtain masses of $\sim 2\text{--}4.5 \times 10^{15} M_\odot$. This is comparable to a massive cluster. From the Mass-Luminosity and Mass-Temperature relations measured for galaxy clusters, we would expect a system of this mass to have an X-ray luminosity of $\sim 10^{45} \text{ erg s}^{-1}$ and a temperature $\sim 10 \text{ keV}$ (Reiprich & Böhringer 2002; Sanderson et al. 2003). Clearly this strongly indicates that the system is not truly bound. It seems more likely that IC 1531 lies in a region where a galaxy group will form in future, perhaps as part of a filament between larger scale galaxy structures.

5 DISCUSSION

As discussed in the previous section, all three of the galaxies observed appear to be in quite sparse environments, with much lower galaxy densities than those found in the cores of groups and clusters. Our examination of the environment of NGC 4555 (in OP04) found it to be in an environment similar to that of IC 1531. Both galaxies are isolated by our criteria, and are not part of any larger virialized system, but have a sufficient number of low luminosity neighbours that it seems likely that they are in regions where groups may form in future. NGC 57 and NGC 7796 are even more isolated, with only a handful of small neighbours. The very low densities of their environments suggest that they may never become part of a galaxy group. In all cases it seems very unlikely that the development of our target galaxies has been affected by interactions with neighbouring objects. We therefore feel secure in considering them as isolated, individual systems. Given the similarity of their environments, and therefore the possibility of similarity in their formation histories, the variation in their properties is interesting.

5.1 Galactic winds vs. hydrostatic haloes

NGC 4555 and NGC 57 both have extended X-ray haloes, detectable to $\sim 50\text{--}60 \text{ kpc}$, containing $\sim 10^{10} M_\odot$ of gas within this radius, and with temperatures of $\gtrsim 1 \text{ keV}$. M/L ratio profiles for these two galaxies fall to values similar to those expected for stars alone ($5\text{--}8 M_\odot/L_{B\odot}$) at small radii, but there is no strong indication of deviations from hydrostatic equilibrium. Given the short cooling times in the cores of the two galaxies, and the evidence from surface brightness and spectral fitting of central point sources and powerlaw spectra, there is the possibility that cooling is being balanced by low-power AGN activity. In this case we might expect some deviation from hydrostatic equilibrium. However, seems to be a relatively minor effect, and we consider it unlikely that our estimated mas profiles for these two systems have been significantly effected, particularly at large radius.

In contrast, NGC 7796 and IC 1531 both have somewhat cooler ($\sim 0.5 \text{ keV}$) and in the case of IC 1531 more compact haloes, and the estimated total M/L ratio profile of NGC 7796 drops below the expected stellar M/L ratio within $\sim 10 \text{ kpc}$. Given the disagreement with the Bertin et al. M/L profile based on stellar velocity dispersion measurements, this suggests that the halo is not in hydrostatic equilibrium, at least in the central part of the galaxy. One possibility is that the gas in NGC 7796 is in a wind state, with supernovae heating the gas and producing significant motions (e.g. Pellegrini & Ciotti 1998; Ciotti et al. 1991). Galaxy winds can have a range of structures depending on parameters such as SN heating rate, galaxy mass and density profile. In the case of NGC 3379, an elliptical where the X-ray mass estimate is observed to be low compared to dynamical estimates, wind models have been applied to show that a galaxy wind can produce a mass underestimate of a factor ~ 2 within the effective radius (Pellegrini & Ciotti 2006). An underestimate of a factor of 2-3 is required to bring our X-ray mass measurements into line with the dynamical estimate. The 0.5 keV temperature of NGC 7796 is quite typical of that expected from a wind system. It is also notable that the modelling of NGC 3379 shows that the mass discrepancy rises to a peak at small radii, perhaps providing an explanation for the low values of M/L we observe in the inner regions. Without detailed modelling of NGC 7796 it is difficult to judge the reliability of the mass profile.

The presence of an AGN and extended radio source in IC 1531 is interesting, in that it raises the question of interaction between the AGN jet and the gaseous halo. We estimate the total radio power of the source to be $L_{\text{Radio}} = 6.6 \times 10^{41} \text{ erg s}^{-1}$ (10 MHz-10 GHz) based on the measurements of Ekers et al. (1989). The X-ray luminosity is similar, $\sim 2.9 \times 10^{41} \text{ erg s}^{-1}$ in the $0.4\text{--}7.0 \text{ keV}$ band. The radio luminosity is comparable to that of some cluster central galaxies; M87 has $L_{\text{Radio}} = 7.5 \times 10^{41} \text{ erg s}^{-1}$. We can roughly estimate the mechanical power output of the radio jets from the relation of Birzan et al. (2004), and find $L_{\text{mech}} = 1.24 \times 10^{43} \text{ erg s}^{-1}$. Comparison with the luminosity of the gaseous halo shows that $\sim 1\%$ of this energy would be sufficient to counteract radiative cooling. This suggest that either IC 1531 is in the process of losing its halo through AGN heating and evaporation (this should take no more than a few 10^7 yr), or that the jets have cleared channels through the halo we observe and now deposit very little energy in the gas.

Based on the global spectral fit and surface brightness modelling of IC 1531 we estimate the gas mass within $30''$ of the galaxy core to be $5.96^{+6.07}_{-2.16} \times 10^8 M_\odot$ (1σ uncertainties). The large errors on the best fitting value are driven by the uncertainty in the relative normalisations of the plasma and powerlaw models. While the upper end of this range is comparable with NGC 4555

and NGC 57, the best fitting value is similar to that found in NGC 7196 at the same physical radius. Given the compactness of the halo, it seems likely that the AGN activity has expelled some gas from the system already and that the halo is not in undisturbed hydrostatic equilibrium. It is possible that IC 1531 also hosts a supernova driven galactic wind. The time taken to accumulate the observed gas mass can be estimated based on a present day stellar mass loss rate from asymptotic giant branch stars of $\dot{M}_* = 0.078(L_B/10^{10}L_{B\odot}) M_{\odot} \text{ yr}^{-1}$, comparable to the stellar mass loss rates derived from *Infrared Space Observatory* observations of nine ellipticals (Athey et al. 2002). From this rate, we estimate that $\sim 10^9$ yr are required to build up the current gas content. We estimate the cooling time in the outer part of the halo to be $\sim 3 \times 10^9$ yr, suggesting that stellar mass loss is introducing new gas faster than cooling can remove it.

AGN heating could also be partially or largely responsible for driving such a wind. As mentioned above, only a few per cent of the likely energy output of the jet would be sufficient to significantly heat the gas and potentially produce a global outflow. Alternatively, the halo might have been truncated by AGN heating. It has been suggested that in some systems energy may be deposited at the point where jets cease to be tightly collimated, leading to the heating and removal of the outer part of the halo while the inner region remains unaffected (Sun et al. 2005a,b). It is possible that IC 1531 has lost gas in this way, with the jets stripping away the outer halo but leaving some gas in the inner core. Jet/gas interactions might be expected to produce structure in the halo via shocks or compression of the gas. We see no indication of such structures, or of strong asymmetries in the halo, but we note that outside the central $7.5''$ where the X-ray jet dominates, only ~ 300 counts (0.3–1.5 keV) are detected by *Chandra*, making assessment of the halo morphology difficult. Higher resolution radio observations might provide further indications of the current relationship between the jet and gas, and show over what range the jets remain collimated.

5.2 Comparison with mass estimates for other early-type galaxies

As mentioned in § 1, the dark matter content of elliptical galaxies is currently a subject of debate. A number of mechanisms have been used to estimate mass profiles in ellipticals, but each suffers from potential issues which can affect the accuracy of the result. Gravitational lensing, perhaps the most direct way of measuring mass, is capable of tracing the mass profile out to $\sim 100r_e$ (e.g. Gavazzi et al. 2007). However, it relies on stacking multiple galaxies to produce the required signal-to-noise and so provides information on the average properties of the population rather than on individual systems and the differences between them.

Kinematic modelling using stellar, globular cluster (GC) and planetary nebula (PN) velocities provides another mechanism for measuring mass profiles. Mass measurements based on stellar velocity dispersions are limited to relatively small radii by the decreasing surface brightness of the stellar population, but the inclusion of PNe or GCs can extend profiles out to ~ 5 – $10 r_e$. Unfortunately a number of factors can affect the accuracy of the kinematic models used. For example, models of merging disc galaxies suggest that the merger process may produce a population of stars on very radial orbits (Dekel et al. 2005). In the early-type galaxy which results from the merger, this population of stars will produce a large number of the PNe observed at large radii, introducing a bias which must be accounted for in any mass models. It has been suggested that early results based on PNe modelling which found low

DM content (Romanowsky et al. 2003) could be affected by this problem, though it may not explain all of the discrepancy between observations and predictions (Dekel et al. 2005; Mamon & Łokas 2005b). The large numbers of tracers (GCs or PNe) required to characterise the anisotropy of the velocity distribution renders this technique difficult for many systems, particularly those with sparse GC/PN populations.

Napolitano et al. (2005) provide a collection of mass profiles based on kinematical modelling in 21 nearby ellipticals. They find the typical M/L ratio at $0.5r_e$ to be $\sim 7M_{\odot}/L_{B\odot}$, providing a good measure of the typical M/L of the stellar population with minimal DM contribution, though in some systems values as low as ~ 3 are reported. The outer radius to which the M/L ratio can be traced varies with the study, and there is considerable variation between galaxies, with some systems showing no evidence of an increase in M/L (e.g. NGC1379, NGC4697). There is some indication that the most optically luminous galaxies are also the most dark matter dominated, with some fainter ellipticals showing little evidence for massive DM haloes. The authors suggest that this may be evidence for haloes with lower central concentrations than predicted by standard Λ CDM models. For comparison with our isolated ellipticals we consider the M/L ratio at $\sim 5r_e$. This is the approximate limit of our profiles, and should be large enough to ensure that the dark halo is the dominant mass component, rather than the stellar population. The Napolitano et al. sample suggests that a M/L ratio of 20 – $30M_{\odot}/L_{B\odot}$ at this radius is fairly typical of the more luminous galaxies. The Napolitano et al sample contains only one galaxy of comparable isolation to the three systems discussed in this paper, NGC 821, which has a M/L ratio of $13.1 \pm 3.9 M_{\odot}/L_{B\odot}$ at $4.8r_e$. Unfortunately it has almost no hot gas content (Pellegrini et al. 2007), so a direct X-ray comparison is not possible.

The number of available mass estimates from X-ray data has improved greatly since we reviewed this area in OP04. The most notable additions are the studies of Fukuzawa et al. (2006), who analysed data for 53 elliptical galaxies drawn from the *Chandra* and *XMM* archives, and Humphrey et al. (2006) who performed a detailed study of seven ellipticals chosen to have relaxed haloes. Fukuzawa et al. report values of 5 – $80M_{\odot}/L_{B\odot}$ at $5r_e$ with variations of at least one order of magnitude between galaxies at all radii. Their M/L ratio profiles show a correlation with the size and luminosity of the X-ray halo, with some faint, compact systems showing M/L ratios as low as $2 M_{\odot}/L_{B\odot}$. They also find an increased scatter in the profiles at small radius. Humphrey et al. find M/L ratios of ~ 7 – $25M_{\odot}/L_{B\odot}$ at $5r_e$. All seven systems have M/L profiles which rise with radius, indicating the presence of a dark halo.

As is to be expected, there are issues which require consideration when interpreting these results. The association of low X-ray luminosity with systems of low M/L ratio, found by Fukuzawa et al., could be explained by those galaxies hosting galactic winds rather than hydrostatic haloes. If this is the case, then the low M/L values found for the compact systems would be incorrect, owing to an underestimation of the total mass. The large variation in M/L at small radii may be the product of AGN heating, which is likely to have the largest effect on the pressure and temperature of the interstellar medium (ISM) in the galaxy core. Although Humphrey et al. selected their galaxies to have relaxed haloes, it is notable that they find their lowest M/L ratio, highest stellar M/L ratio, highest virial mass and lowest DM halo concentration for NGC 4261, an FR-I radio galaxy with radio and X-ray jets which extend to $\gtrsim 3.5r_e$ (Zezas et al. 2005). Fitting the mass profile with a model consisting

of stellar and DM components, Humphrey et al. find that the stars dominate the mass profile out to $\sim 6r_e$ (~ 20 kpc). While it is possible that the galaxy does indeed have such a low density of dark matter in its inner regions, it also seems possible that jet heating and disturbance of the inner halo could have affected the estimated mass profile. The two samples also contain galaxies from a range of environments, ranging from field galaxies to those in nearby clusters and a large number of group dominant ellipticals. While this may not affect the mass profile within a few r_e , it suggests that caution should be employed when considering results at large radii, where contributions from the dark matter halo of any surrounding system need to be considered.

The Humphrey et al. and Fukuzawa et al. samples also contain two fairly isolated galaxies, NGC 720 and NGC 6482. The latter was originally selected as a fossil group candidate, and *Chandra* observations show the halo to be luminous and extended, providing a degree of support for this classification (Khosroshahi et al. 2004). However, Buote et al. argue that the total system mass is significantly lower than groups such as NGC 5044 and that NGC 6482 should be considered as an isolated elliptical. Unfortunately a detailed study of the galaxy population around NGC 6482, which might resolve the issue, is not yet available, making a definitive classification difficult. NGC 720 is also a borderline object; it has been identified as the dominant elliptical of the LGG 38 group (Garcia 1993) but the other members of the group are all considerably fainter. NGC 720 would meet our selection criteria for isolated galaxies were it not for its prior identification as a group. Buote et al. argue that the mass of the system is too low to represent a galaxy group, and its reported X-ray luminosity falls below the minimum required for fossil groups. However, an examination of the local surface density of galaxies with no measured redshift (as performed for NGC 7796 and NGC 57 in § 4) suggests that there may be a significant excess of galaxies around NGC 720. This could indicate that the galaxy is in fact part of a fossil group-like system, but more detailed studies are required for a definitive judgment. For comparison with our galaxies, we note that both systems may fall in the category of isolated ellipticals, but that both appear to be in rather denser environments than any of our targets.

Our mass profile for NGC 57 only extends to $4.75r_e$, at which point the M/L ratio is $44.7^{+4.0}_{-8.5} M_\odot/L_{B\odot}$ (1σ uncertainties). From OP04 the value for NGC 4555 at $5r_e$ is $43.2^{+15.2}_{-21.6} M_\odot/L_{B\odot}$ and for NGC 7796 (assuming hydrostatic equilibrium) $10.6^{+2.5}_{-2.3} M_\odot/L_{B\odot}$. It is clear that at this radius, NGC 57 and NGC 4555 are quite similar, and are fairly massive systems with considerable DM content. Their M/L ratios are rather higher than the dynamical estimates given by Napolitano et al. for systems of similar *B*-band luminosity. However, the uncertainties on our estimates are large enough that the differences are not strongly significant, particularly in the case of NGC 4555. In any case the mass profile of NGC 57 strongly indicates the presence of a fairly massive dark halo, lending weight to the result of OP04 that individual ellipticals can possess significant quantities of DM regardless of environment.

Humphrey et al. suggest that NGC 4555 may possess a group-scale dark halo and have formed through a process similar to that of a fossil group. The velocity dispersions of NGC 4555 (350 km s^{-1} , Wegner et al. 2003) and NGC 57 ($\sim 326 \text{ km s}^{-1}$, LEDA) are rather higher than those of IC 1531 and NGC 7796 (226 and 260 km s^{-1} respectively). Both NGC 57 and NGC 4555 fall at the upper end of the $\sigma:T_X$ relation for ellipticals (Fukazawa et al. 2006; O’Sullivan et al. 2003), having parameters comparable to many group dominant ellipticals. This could be an indication of the presence of group-scale dark matter halos. From a technical viewpoint,

both NGC 4555 and NGC 57 fail to meet the criteria for classification as a fossil group. Although both galaxies meet our isolation criteria, neither is quite as isolated as is usually required for a fossil group (no neighbours less than 2 magnitudes fainter within 2000 km s^{-1} and 1 Mpc). However, this does not rule out the possibility that these could be galaxies in a group-sized DM halo which have formed by multiple mergers at an early epoch. Both galaxies are fainter than the minimum luminosity of $10^{42} \text{ erg s}^{-1}$ used to select fossil groups, and neither X-ray halo is as extended as would be expected for a group-scale object. It is difficult to see how a group-scale system which formed rapidly at an early epoch could have such a low X-ray luminosity. We would expect a halo with a X-ray luminosity and gas content similar to any normal group; as there is no evidence of excessive star formation, we would have to assume that the group had somehow lost $\sim 80\text{--}95$ per cent of its gas content through evaporation, a very extreme scenario. This argument does not rule out a fossil group-like formation mechanism, though it does suggest that the total mass of these galaxies is likely to be considerably lower than that of such groups.

More detailed mass modelling, which given the distance of these two systems requires deeper X-ray observations, could provide insight into the relationship of these galaxies to fossil groups. Similarly, measurement of the local galaxy luminosity functions could determine whether NGC 4555 and NGC 57 have the large population of gravitationally bound satellite galaxies expected in a fossil group. An argument against a fossil group-type formation history for these systems is the relatively flat galaxy surface density profiles shown in Figures 7 and 8, which suggest the presence of only a few small neighbouring galaxies. However, better optical data is required if this issue is to be resolved. Perhaps a stronger argument that the formation mechanism of isolated ellipticals is not the same as that of fossil groups is that a significant number of systems studied in the optical show signs of recent mergers or interactions (Reda et al. 2004). However, further investigation of this area is required to determine how isolated ellipticals form, and whether there is a continuum of properties, with fossil groups as the more luminous counterparts of the systems considered here.

The lower M/L found for NGC 7796 suggests that it is considerably less massive than NGC 57 and NGC 4555, if we assume it to be in hydrostatic equilibrium. It is comparable with several of the ellipticals with lower optical luminosities in the Napolitano et al. sample, including NGC 821, which is similarly isolated. This emphasizes the difference between NGC 7796 and NGC 57, which has a near-identical optical luminosity. A number of possibilities could explain the low value found for this system. If we assume that the mass profile we measure is accurate, at least in the outer part of the galaxy, then we must assume either that NGC 7796 has only a minimal dark matter halo, or that its halo has a relatively large core and that we do not trace the mass profile far enough to see the rise in M/L ratio. The latter scenario could suggest either a deviation from the expected NFW DM profile, as is suggested by Napolitano et al. to explain the lower mass systems in their sample, or possibly a low concentration NFW halo, as found by Humphrey et al. for NGC 4261. However, the very low M/L ratio found in the centre of NGC 7796 suggests that our mass profile may well be unreliable in the galaxy core, and in this circumstance we must consider the possibility that the halo as a whole is not in hydrostatic equilibrium, but is in a galactic wind state.

6 SUMMARY AND CONCLUSIONS

We have used *Chandra* and *XMM-Newton* to observe three isolated early-type galaxies, NGC 57, IC 1531 and NGC 7796. All three appear to be in very low density environments with few neighbouring galaxies of comparable mass. None of the three is part of a larger virialized system, though there is some indication that IC 1531 is in a region in which a poor group may form in the future. The three galaxies have a range of X-ray properties. NGC 57 has an extended halo of ~ 0.9 keV, roughly solar metallicity gas. IC 1531 is a radio galaxy and its X-ray emission is dominated by the AGN and an associated jet, with only a compact, cooler (~ 0.5 keV) halo. NGC 7796 has no strong AGN, and possesses a halo with a similar temperature to that of IC 1531, but which is more extended.

For each galaxy we model the surface brightness and temperature distributions of the gas haloes. In IC 1531 the compactness of the halo and the strength of the AGN contribution limits us to two radial temperature bins, but three and four bins are used for NGC 57 and NGC 7796 respectively. All three galaxies are consistent with having isothermal temperature profiles, though there is some evidence of a slight drop in the central temperature of NGC 57. For NGC 7796 and NGC 57 we use these measurements to estimate the gas content, cooling time and entropy of the haloes and perform a comparison with NGC 4555, another elliptical detailed in a previous paper. The three galaxies have similar entropy and cooling time profiles, but NGC 7796 has a slightly lower gas mass at all radii.

We also estimate the total mass and mass-to-light ratio profiles of NGC 57 and NGC 7796, and find that NGC 57 has very similar properties to NGC 4555; both galaxies have fairly massive dark haloes. The M/L ratio of NGC 57 at $4.75r_e$ is found to be $44.7_{-8.5}^{+4.0} M_{\odot}/L_{B\odot}$ (1σ uncertainties). This demonstrates that NGC 4555 is not a unique system, and strongly suggests that elliptical galaxies can possess moderately massive dark haloes independent of larger-scale systems. At present NGC 4555 and NGC 57 are the two most isolated ellipticals with accurate X-ray mass profiles, and NGC 821 is the only comparably isolated galaxy with a dynamical mass estimate. NGC 7796 has a lower total mass and M/L ratio at any given radius, with a M/L of $10.6_{-2.3}^{+2.5} M_{\odot}/L_{B\odot}$ at $5r_e$. This may indicate that the dark matter halo of the galaxy is not as massive as that of NGC 57, or the structure of their DM their profiles differ. However, very low M/L ratios are found in the core of the galaxy, and this may indicate that our X-ray-derived mass is unreliable because the gas is not in hydrostatic equilibrium, perhaps because it takes the form of a galactic wind. Comparison with other X-ray and dynamical mass estimates shows a number of systems with values comparable to those found for our galaxies, but also reveals a number of factors which may have biased the results. Cross-comparison of mass estimates for the same object using independent techniques seems the mostly likely way to resolve these issues.

acknowledgments

We thank the referee, Y. Fukazawa, for comments which have materially improved the paper. Support for this work was provided by the National Aeronautics and Space Administration through NASA Grants NNG04GF19G and NNG05GI62G, and through Chandra Award Numbers G05-6129X and G06-7070X-R issued by the Chandra X-ray Observatory Center, which is operated by the Smithsonian Astrophysical Observatory for and on behalf of the National Aeronautics Space Administration under contract NAS8-03060. AJRS also acknowledges support from PPARC. This research made use of the NASA/IPAC Extragalactic Database (NED)

which is operated by the Jet Propulsion Laboratory, California Institute of Technology, under contract with the National Aeronautics and Space Administration, the Digitized Sky Surveys (DSS), produced at the Space Telescope Science Institute under U.S. Government grant NAG W-2166, NASA's Astrophysics Data System, and the HyperLeda database (<http://leda.univ-lyon1.fr>).

REFERENCES

- Acreman D. M., Stevens I. R., Ponman T. J., Sakelliou I., 2003, *MNRAS*, 341, 1333
- Anders E., Grevesse N., 1989, *Geo. et Cosmo. Acta*, 53, 197
- Arnaut M., Majerowicz S., Lumb D., Neumann D. M., Aghanim N., Blanchard A., Boer M., Burke D. J., Collins C. A., Giard M., Nevalainen J., Nichol R. C., Romer A. K., Sadat R., 2002, *A&A*, 390, 27
- Athey A., Bregman J., Bregman J., Temi P., Sauvage M., 2002, *ApJ*, 571, 272
- Bacon R., Monnet G., Simien F., 1985, *A&A*, 152, 315
- Bahcall J. N., Tremaine S., 1981, *ApJ*, 244, 805
- Barnes J. E., 1989, *Nature*, 338, 123
- Bertin G., Bertola F., Buson L. M., Danzinger I. J., Dejonghe H., Sadler E. M., Saglia R. P., de Zeeuw P. T., Zeilinger W. W., 1994, *A&A*, 292, 381
- Birzan L., Rafferty D. A., McNamara B. R., Wise M. W., Nulsen P. E. J., 2004, *ApJ*, 607, 800
- Buote D., Fabian A., 1998, *MNRAS*, 296, 977
- Buote D. A., 2000, *MNRAS*, 311, 176
- Cash W., 1979, *ApJ*, 228, 939
- Ciotti L., D'Ercole A., Pelegrini S., Renzini A., 1991, *ApJ*, 376, 380
- Colless M., Dalton G., Maddox S., Sutherland W., Norberg P., Cole S., Bland-Hawthorn J., Bridges T., Cannon R., Collins C., Couch W., Cross N., Deeley K., et al. 2001, *MNRAS*, 328, 1039
- Dekel A., Stoehr F., Mamon G. A., Cox T. J., Primack J. R., 2005, *Nature*, 437, 707
- Diehl S., Statler T. S., 2006, *ArXiv Astrophysics e-prints*, astro-ph/0606215
- Douglas N. G., Napolitano N. R., Romanowsky A. J., Coccatto L., 2007, *ApJ*, submitted
- Dressler A., 1980, *ApJ*, 236, 351
- Ekers R. D., Wall J. V., Shaver P. A., Goss W. M., Fosbury R. A. E., Danziger I. J., Moorwood A. F. M., Malin D. F., Monk A. S., Ekers J. A., 1989, *MNRAS*, 236, 737
- Forman W., Jones C., Tucker W., 1985, *ApJ*, 293, 102
- Freedman W. L., Madore B. F., Gibson B. K., Ferrarese L., Kelson D. D., Sakai S., Mould J. R., Kennicutt Jr. R. C., Ford H. C., Graham J. A., Huchra J. P., Hughes S. M. G., Illingworth G. D., Macri L. M., Stetson P. B., 2001, *ApJ*, 553, 47
- Fruscione A., McDowell J. C., Allen G. E., Brickhouse N. S., Burke D. J., Davis J. E., Durham N., Elvis M., Galle E. C., Harris D. E., Huenemoerder D. P., Houck J. C., et al. 2006, in *Observatory Operations: Strategies, Processes, and Systems*. Edited by Silva, David R.; Doxsey, Rodger E.. Proceedings of the SPIE, Volume 6270, pp. (2006). CIAO: Chandra's data analysis system
- Fukazawa Y., Botoya-Nonesca J. G., Pu J., Ohto A., Kawano N., 2006, *ApJ*, 636, 698
- Garcia A. M., 1993, *A&AS*, 100, 47
- Gavazzi R., Treu T., Rhodes J. D., Koopmans L. V. E., Bolton A. S., Burles S., Massey R. J., Moustakas L. A., 2007, *ArXiv Astrophysics e-prints*, astro-ph/0701589

- Grevesse N., Sauval A. J., 1998, *Space Sci. Rev.*, 85, 161
- Helsdon S. F., Ponman T. J., O'Sullivan E., Forbes D. A., 2001, *MNRAS*, 325, 693
- Humphrey P. J., Buote D. A., Gastaldello F., Zappacosta L., Bullock J. S., Brighenti F., Mathews W. G., 2006, *ApJ*, 646, 899
- Jansen F., Lumb D., Altieri B., Clavel J., Ehle M., Erd C., Gabriel C., Guainazzi M., Gondoin P., Much R., Munoz R., Santos M., Schartel N., Texier D., Vacanti G., 2001, *A&A*, 365, L1
- Jensen J. B., Tonry J. L., Barris B. J., Thompson R. I., Liu M. C., Rieke M. J., Ajhar E. A., Blakeslee J. P., 2003, *ApJ*, 583, 712
- Jones L. R., Ponman T. J., Horton A., Babul A., Ebeling H., Burke D. J., 2003, *MNRAS*, 343, 627
- Kellogg E., Baldwin J. R., Koch D., 1975, *ApJ*, 199, 299
- Khosroshahi H. G., Jones L. R., Ponman T. J., 2004, *MNRAS*, 349, 1240
- Mamon G. A., Łokas E. L., 2005a, *MNRAS*, 362, 95
- Mamon G. A., Łokas E. L., 2005b, *MNRAS*, 363, 705
- Mathews W. G., Brighenti F., 2003, *ARA&A*, 41, 191
- Melnick J., Sargent W. L. W., 1977, *ApJ*, 215, 401
- Milone A. d. C., Rickes M. G., Pastoriza M. G., 2007, *A&A*, 469, 89
- Napolitano N. R., Capaccioli M., Romanowsky A. J., Douglas N. G., Merrifield M. R., Kuijken K., Arnaboldi M., Gerhard O., Freeman K. C., 2005, *MNRAS*, 357, 691
- O'Sullivan E., Forbes D. A., Ponman T. J., 2001, *MNRAS*, 328, 461
- O'Sullivan E., Ponman T. J., 2004, *MNRAS*, 354, 935, OP04
- O'Sullivan E., Ponman T. J., Collins R. S., 2003, *MNRAS*, 340, 1375
- O'Sullivan E., Vrtilek J. M., Harris D. E., Ponman T. J., 2007, *ApJ*, 658, 299
- O'Sullivan E., Vrtilek J. M., Kempner J. C., David L. P., Houck J. C., 2005, *MNRAS*, 357, 1134
- Paturel G., Petit C., Prugniel P., Theureau G., Rousseau J., Brouty M., Dubois P., Cambrésy L., 2003, *A&A*, 412, 45
- Pellegrini S., Baldi A., Kim D. W., Fabbiano G., Soria R., Siemiginowska A., Elvis M., 2007, *ArXiv Astrophysics e-prints*, astro-ph/0701639
- Pellegrini S., Ciotti L., 1998, *A&A*, 333, 433
- Pellegrini S., Ciotti L., 2006, *MNRAS*, 370, 1797
- Ponman T. J., Bertram D., 1993, *Nature*, 363, 51
- Pratt G. W., Arnaud M., Aghanim N., 2001, in Neumann D. M., Tranh Thanh Van J., eds, *Clusters of Galaxies and the High Redshift Universe Observed in X-rays: XMM-Newton observations of galaxy clusters; the radial temperature profile of A2163*
- Reda F. M., Forbes D., Hau G. T. K., 2005, *MNRAS*, 360, 693
- Reda F. M., Forbes D. A., Beasley M. A., O'Sullivan E. J., Goudfrooij P., 2004, *MNRAS*, 354, 851
- Reiprich T. H., Böhringer H., 2002, *ApJ*, 567, 716
- Romanowsky A. J., Douglas N. G., Arnaboldi M., Kuijken K., Merrifield M. R., Napolitano N. R., Capaccioli M., Freeman K. C., 2003, *Science*, 301, 1696
- Sanderson A. J. R., Ponman T. J., Finoguenov A., Lloyd-Davies E. J., Markevitch M., 2003, *MNRAS*, 340, 989
- Smith R. K., Brickhouse N. S., Liedahl D. A., Raymond J. C., 2001, *ApJ*, 556, L91
- Smith R. M., Martínez V. J., Graham M. J., 2004, *ApJ*, 617, 1017
- Spergel D. N., Bean R., Dore' O., Nolta M. R., Bennett C. L., Hinshaw G., Jarosik N., Komatsu E., Page L., Peiris H. V., Verde L., Barnes C., Halpern M., et al. 2007, *ApJS*, 170, 377
- Sun M., Jerius D., Jones C., 2005, *ApJ*, 633, 165
- Sun M., Vikhlinin A., Forman W., Jones C., Murray S. S., 2005, *ApJ*, 619, 169
- Thomas D., Maraston C., Bender R., Mendes de Oliveira C., 2005, *ApJ*, 621, 673
- Tonry J. L., Dressler A., Blakeslee J. P., Ajhar E. A., Fletcher A. B., Luppino G. A., Metzger M. R., Moore C. B., 2001, *ApJ*, 546, 681
- Trinchieri G., Fabbiano G., Canizares C. R., 1986, *ApJ*, 310, 637
- Tully R. B., 1987, *ApJ*, 321, 280
- Voit G. M., Donahue M., 2005, *ApJ*, 634, 955
- Wegner G., Bernardi M., Willmer C. N. A., da Costa L. N., Alonso M. V., Pellegrini P. S., Maia M. A. G., Chaves O. L., Rité C., 2003, *AJ*, 126, 2268
- Weisskopf M. C., Brinkman B., Canizares C., Garmire G., Murray S., Van Speybroeck L. P., 2002, *PASP*, 114, 1
- Zezas A., Birkinshaw M., Worrall D. M., Peters A., Fabbiano G., 2005, *ApJ*, 627, 711